Bitopic inhibition of ATP and substrate binding in Ser/Thr kinases through a conserved allosteric mechanism

Ning Ma[1], Lisa G. Lippert[2], Titu Devamani[2], Benjamin Levy[1], Sangbae Lee[1], Manbir Sandhu[1], Nagarajan Vaidehi[1,*] and Sivaraj Sivaramakrishnan[2,*]

[1] Department of Computational and Quantitative Medicine, Beckman Research Institute of the City of Hope, Duarte, CA 91010

[2] Department of Genetics, Cell Biology, and Development, University of Minnesota, Minneapolis, MN 55455

Supporting Information

Methods

1. Computational Methods

1.1 Preparation of kinase catalytic domain structures for MD simulations – The crystal structure of the activated state of the catalytic domain of PKCα (PDB ID 3IW4)[1] was used as a starting structure for the MD simulations. However, this structure was missing the activation loop and the C-terminus. We modeled the activation loop into this structure using MODELLER[2] using the PKCβII crystal structure as the template (PDB ID: 3PFQ).[3] The C-terminus was also built in using MODELLER with the crystal structure of PKCα PDB ID: 4RA4.[4] We used the 3IW4 as the starting structure since this had the least number of missing residues. The three residues that are phosphorylated in the active form PKCα (Thr494, Thr638 and Ser657) were modified to the phosphorylated form in this study. The generated structure was minimized by Macromodel application, Maestro software suite (Schrödinger Release 2018-2: Maestro, Schrödinger, LLC, New York, NY, 2018.), with a maximum of 5000 steps, or until convergence of 0.05 kcal/mol-Å^2 in force was reached. We used the following crystal structures as starting structures for the MD simulations of other kinases: AKT (PDB ID: 3QKK),[5] STK40 (PDB ID: 5L2Q),[6] PDK1 (PDB ID: 1OKY),[7] ABL (PDB ID: 4WA9).[8] The simulations for these kinases were performed with no ligand or substrate bound, and also in non-phosphorylated form. The D481 or equivalent residue in all kinases mentioned above were mutated to Alanine in Maestro, followed by a 5,000 steps of minimization to optimized the side chain orientation of Alanine, while keeping all other residues fixed. The minimized structures were kept as initial structures for mutant-system simulations. Sequences alignment shown in Fig. 1D was performed using Clustal Omega provided by EMBL-EBI.[9]

Five inhibitors, BimI, sotrastaurin, staurosporine, sangivamycin and toyocamycin, were docked into the ATP binding pocket of PKCα using Glide SP, flexible ligand docking. Ligand and protein van der Waals radii were scaled by 0.5, and a clash score greater than 100 kcal/mol in combined van der Waals and Coulombic interaction energy was used as to reject docked poses. The best docked poses were those showing lowest interaction energy, and correct orientation and alignment of ligand functional groups with those identified in crystal structures of the ligand with other kinases. The key interaction between these inhibitors and residues around the binding pocket were already identified in PKCα or other kinases from previous crystal structures.[10–12] These inhibitors were known to interact with residues V420 and D467 (sotrastaurin/staurosporine, template PDB ID 3IW4/1XJD)[10,11] or D481 (BimI, template PDB ID 2VD5)[12] in PKC. The docked conformation that most similar to original crystal binding conformation were further optimized by performing Prime rigid body minimization of the ligand within the PKCα catalytic site, followed by three rounds of Prime sidechain reassignment was used to optimize the sidechain packing of the residues within 5 Å around the ligand. In each of the three rounds, sidechains within 5 Å of the ligand were optimized, beginning first with aromatic residues phenylalanine, tyrosine, and tryptophan. The second round consisted of polar residues arginine, lysine, histidine, aspartate, glutamate, asparagine, glutamine, serine, and threonine. The final round of sidechain optimization was performed on hydrophobic residues alanine, cysteine, isoleucine, leucine, methionine, and valine. Inhibitor-PKCα complex structures were then minimized with Macromodel for 5,000 steps or until convergence threshold of 0.05 kcal/mol-Å^2 was reached, and kept as initial structure for inhibitor-protein complex simulations. Similar strategy was applied to acquire binding conformation of ATP, while PKCι-ATP complex crystal structure (PDB ID: 3A8W)[13] was chosen as template to construct PKCα-ATP structure.

1.2 All-atom MD simulations – We performed all-atom MD simulations in explicit solvent for all the PKCα apo-protein and inhibitor complexes. All simulations were performed using GROMACS2016[14] package with GROMOS 54a7 force field.[15] The force field parameters for the phosphate group were adapted from previous 43a1p version.[16] The proteins or inhibitor-protein complexes were solvated in a 90 Å^3 cubic TIP3 water box, and the net charge on the protein neutralized using NaCl. LINCS algorithm was applied on all bonds and angles of waters and a time step of 2 fs was used for integration. Non-bond interactions were calculated with a cut-off of 12 Å, and long range van der Waals interactions were calculated using particle mesh Ewald method.[17] With initial velocities sampled from the Boltzmann distribution, each system was heated slowly to 310 K in NVT ensemble in 1ns, with temperature controlled by Nosé-Hoover thermostat,[18] followed by 30 ns equilibration in NPT ensemble with harmonic position restraints applied on protein and ligand heavy atoms, while pressure coupled to 1 bar and controlled by Parrinello-Rahman method.[19] The restraint force was gradually reduced from 5 kcal/mol-Å^2 to 0 kcal/mol-Å^2 in a 1 kcal/mol-Å^2 per 5 ns window. For the inhibitor-protein complex simulations, flat bottom restraints of 1 kcal/mol-Å^2 were applied between inhibitors and V420 and D467 or D481, to maintain the key interactions during equilibration. These restraints were turned on during the final 5ns equilibration window and were released in the production simulations. For the PKCα-ATP complex system, a Na^+ ion was placed between the γ-PO_4 group of ATP and side chain of D481, and flat bottom restraint potentials were applied between γ-PO_4 - Na^+- D481 side chain, separately. These restraints were applied to maintain the salt bridge between ATP-Na^+-D481 as seen in the crystal structure, and released using the same procedure described above. The force field parameters for inhibitors were prepared by PRODRG server,[20] the partial charge of each atom was replaced by the ESP (atomic electrostatic potential) charge calculated using Hartree-Fock method with Poisson-Boltzmann function for water solvation as implemented in the quantum mechanics software suite Jaguar.[21] We used the 6-31G** basis set to calculate the ESP charges. The last frame after the equilibration step were taken for each system to spin off five independent 200 ns production MD simulations with no restraints and with different initial velocities in the NPT ensemble. A total of 1μs production simulations was performed for each system. Trajectories were saved every 2 ps for further analysis. Analysis and visualization were carried out by GROMACS and VMD.[22]

For each trajectory generated for PKCα, we calculated the root mean square deviation in the coordinates of the backbone atoms from the starting structure and plotted this quantity as a function of time. Fig. S4 shows the RMSD time series plot. The RMSD converges between 3 to 5 Å for the entire catalytic domain of PKCα.

1.3 Calculation of the relative population of the closed to open conformation states – We observed the movement of the activation loop towards the G-loop to form what we term as the "closed" state. We used the distance between centers of mass of backbone atoms of residues from K347 to I349 in the G-loop plus D380, V381 from αC helix, and the residues T495 to C499 in the activation loop to describe the open-closed movement of G-loop and activation loop. K347 to I349 generally move together with D380 and V381 from αC helix, defining them as a group and measure their distance from T495 to C499 group on activation loop can separate closed conformations from open conformations in this work. These residue numbers are for PKCα. For all other kinases simulated in this work we performed a structural alignment of all the structures to PKCα and identified the residues corresponding to K347 to I349, D380-V381 and T495-C499 and used the distance between their centers of mass of the backbone atoms to calculate the ratio of closed to open states. When the MD simulation samples only the open states, the distance histogram distribution plot shows only one peak, when the simulation samples both open and closed states, the distance distribution plot shows two peaks with clear separation. Taking the distance measure at the minimum point between open states peak and closed states peak as a cutoff, the numbers of MD snapshots for each state can be calculated leading to the ratio of closed/open states.

1.4 Calculation of interaction energy of the EGFR peptide substrate with open and closed conformation states – We calculated the interaction energy of the EGFR peptide substrate (amino acid sequence: IVRKATLRRLL) in the open and closed conformation state of PKCα to verify if indeed the open conformation state favors the binding of the peptide substrate as we postulated. We used the EGFR peptide substrate bound PKCα open state structure from our previous study.[23] The initial structure of EGFR peptide bound to the closed state of PKCα was prepared using the following procedure. The closed conformation of PKCα was obtained by performing RMSD based cluster analysis on the 1 μs trajectory of PKCα-BimI complex, and extracting the representative structure from most populated cluster of closed conformation states. We then transferred the EGFR peptide structure from the open conformation state onto substrate binding site with restraining the interaction between R9 residue in the peptide sequence and F498. We then performed 100 cycles of replica exchange annealing torsional molecular dynamics using GNEIMO torsional MD method combined with side chain packing with Rosetta module.[24] The GNEIMO annealing simulations were performed with a harmonic distance restraint applied on R9-F498 to keep the PKCα in the closed state. The representative structure from most populated cluster of EGFR peptide bound closed states of PKCα complex was selected for further all-atom MD simulations. The representative structure of EGFR peptide bound PKCα was used as starting structure for performing five brute force all-atom MD simulations with no restraints each for 200ns totaling to 1 μs simulation time using the same procedure described above. We calculated the non-bond interaction energy between EGFR peptide and the open and closed states of the catalytic domain of PKCα averaged over the entire all-atom MD simulations trajectory. The average interaction energy of the EGFR peptide with open conformation state of PKCα is -1068 ± 88.9 kJ/mol compared to -791±71.0 kJ/mol for the closed conformation state. This analysis suggested that substrate binding will be negatively affected by higher population of the closed state of PKCα.

2. Experimental Methods

2.1 Reagents and Peptides – Buffer ingredients and chemicals were purchased from various commercial vendors and used without further purification. EGFR substrate peptide (sequence – IVRKATLRRLL) was custom-synthesized by GenScript and solubilized in PKC Buffer (20 mM HEPES (pH 7.5), 5 mM $MgCl_2$, 0.5 mM EGTA, and 2 mM DTT).

2.2 Constructs – We used a previously reported SPASM sensor construct containing an alanine-substituted PKCα substrate peptide and the human PKCa catalytic domain.[25] Briefly, human PKCα catalytic domain, mCerulean (FRET donor), mCitrine (FRET acceptor), 10 nm ER/K single α- helix and Ala-substituted substrate peptides, were PCR amplified and cloned into unique restriction sites in the pBiex1 expression vector (Novagen). Gly-Ser-Gly linkers were inserted between protein domains to allow for rotational freedom. Mutant peptides were introduced into sensor by digestion, followed by phosphorylation and ligation of appropriate phosphorylated oligonucleotides. Sanger sequencing was used to confirm appropriate insertion and mutagenesis.

Insect Cell Expression and Protein Purification - Plasmids were transfected into (Sf9) insect cells using a protocol reported previously.[25] Briefly, pBiex1 vectors were transiently transfected into Sf9 insect cells cultured in Sf900- II media (ThermoFisher) using Escort IV transfection reagent (Sigma) and Optimem 1 (ThermoFisher). Cells were harvested (250 g, 5 mins at 4 ºC) and lysed using lysis buffer (20 mM HEPES (pH 7.5), 200 mM NaCl, 4 mM $MgCl_2$, 0.5% sucrose, 0.5% IGEPAL, 2 mM DTT, 50 μg/ml PMSF, 5 μg/ml aprotinin, and 5 μg/ml leupeptin). Clarified lysate after ultracentrifugation (13435 g, 25 mins at 4 ºC) was incubated with anti-FLAG M2 affinity resin (Sigma) for 1-2 hr and washed with wash buffer (20 mM HEPES (pH 7.5), 150 mM NaCl, 10 mM MgCl2, 2 mM DTT, 5 μg/ml PMSF, 5 μg/ml aprotinin and 5 μg/ml leupeptin). The proteins were eluted with FLAG peptide (Sigma, 100 μg/ml) and buffer exchanged to PKC buffer (20 mM HEPES (pH 7.5), 5 mM MgCl2, 0.5 mM EGTA, and 2 mM DTT) using Zeba Spin Desalting Columns (40 kDa, Pierce). Protein concentration for centrifuged protein was determined from the fluorescent emission of mCit (Ex 490, Em 525 nm) compared to a standard on a FluoroMax-4 fluorimeter (Horiba Scientific) or by fluorophore absorbance on a NanoDrop One (ThermoFisher).

2.3 Kinase Activity Assay – Kinase specific activity was inferred from the ATP consumed in phosphorylation reaction using the KinaseGlo Max Luminescence Assay Kit (Promega). ATP depletion is monitored with Kinase-Glo Reagent, which uses luciferin, oxygen and ATP as substrates in a reaction that produces oxyluciferin and light. The luminescent signal is linearly proportional to the amount of ATP remaining following the phosphorylation reaction. Control experiments in which the substrates were incubated with the assay buffer and then assayed with the luciferase showed that substrate/buffer interactions with the luciferase reaction were insignificant under the assay conditions. Activity assays were performed using the catalytic domain (25-75 nM) and 500-μM peptide in PKC Buffer. Reactions were initiated by the addition of 250 μM ATP to a total reaction volume of 80 μL in U-bottom,

white 96-well plates. Following 3 min incubation at 22 °C, the reaction was quenched and subsequent steps were performed as per instructions from the kit provider. End-point luminescence was measured in a FlexStation 3 plate reader (Molecular Devices). Control experiments with only the kinase or the substrate showed negligible ATP consumption. For each experimental condition, ≥ 2 independent measurements were performed for ≥ 3 protein preparations (N ≥ 6).

2.4 FRET Measurements – We have extensively monitored protein-protein interactions in live cells using SPASM FRET sensors.[26–28] FRET measurements provide a direct measure of the binding strength of the substrate peptides to the kinase catalytic domain.[29,30] Before each experiment, purified sensors were centrifuged (17645 g at 4 °C) to remove any insoluble protein. All experiments were performed with 50 nM protein in PKC Buffer at 21-22 °C. Samples were prepared in tubes pre-coated with BSA (0.1 mg/ml) to limit protein loss through adsorption to tube walls. FRET measurements were performed using FluoroMax-4 fluorimeter (Horiba Scientific). Sensor preparations, with and without inhibitors, were loaded in a quartz cuvette (1 cm path length) and excited at 430 nm with an 8-nm band pass, and emission monitored (4-nm band pass) from 450 to 650 nm. The FRET ratio was calculated from the ratio of the emission for mCitrine (525 nm) to mCerulean (475 nm). For each experimental condition, ≥ 2 experimental replicates were measured for ≥ 3 independent protein batches (N ≥ 6).

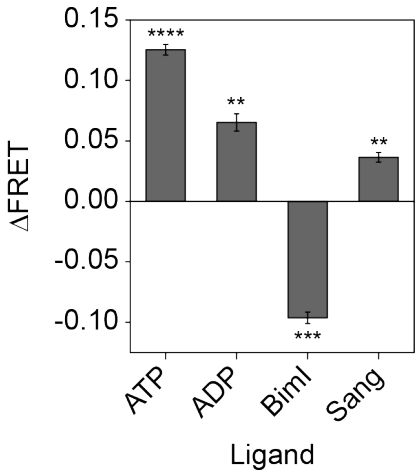

Figure S1: BimI displaces pseudosubstrate from catalytic domain. Change in FRET ratio (ΔFRET) of SPASM sensor that detects interaction between pseudosubstrate peptide (MADVFPGNDSTASQDVANRFARKGALRQKNV) and the catalytic domain of PKCα. Ligand concentrations: 1 uM BimI, 100 uM ATP, 100 uM ADP, 100 uM Sangivamycin. SPASM sensor concentration – 50 nM. Data are standard error of mean from four independent protein preparations. (** = $p<0.01$; *** = $p<0.001$; **** = $p<0.0001$ using a paired t-test relative to no ligand).

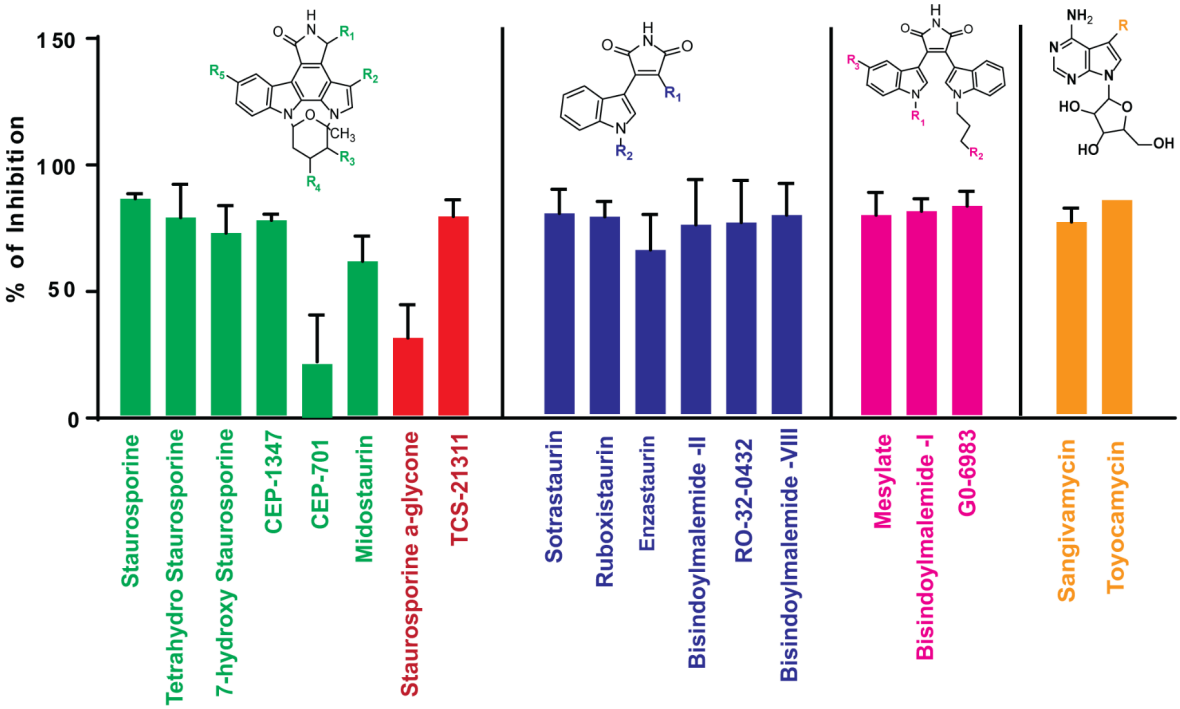

Figure S2: Kinase activity of the isolated PKCα catalytic domain was measured indirectly from the amount of ATP consumed in the phosphorylation reaction (see Methods for details). % inhibition of this kinase activity in the presence of the indicated inhibitors at saturating concentrations (10 μM for all compounds except sangivamycin and toyocamycin which are at 100 μM).

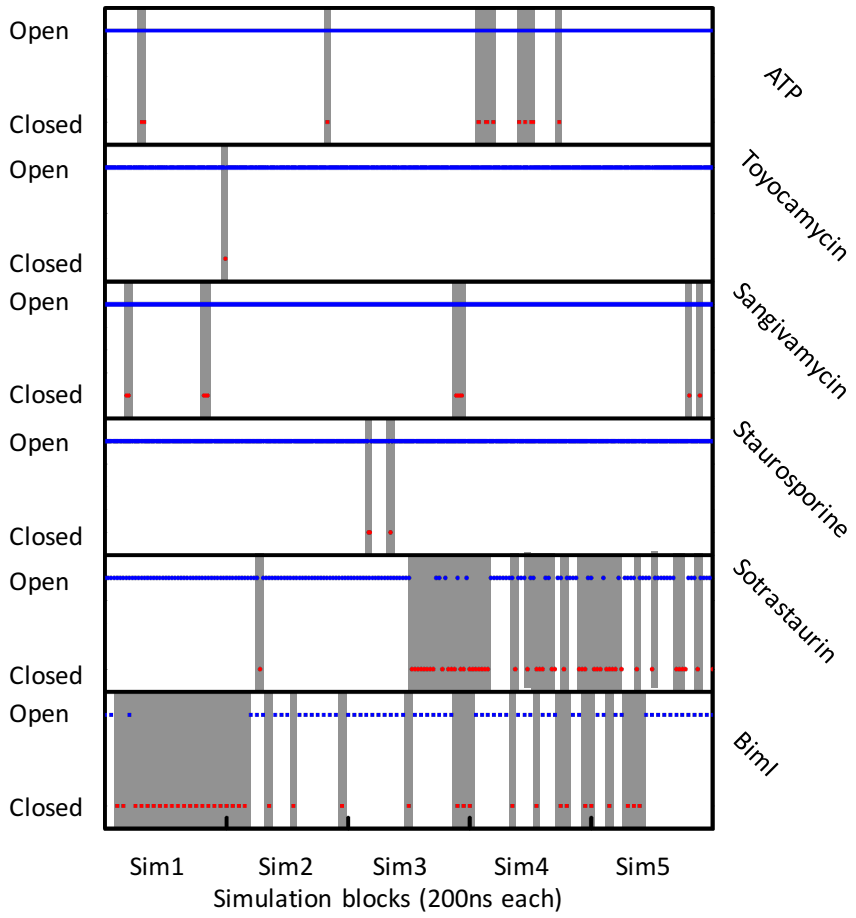

Figure S3: Time series plot of open versus closed state in various inhibitor or ATP bound PKCα. This figure shows the occupation of the open or closed conformation state of the PKCα system with ATP or various inhibitors bound, as a function of time. The results for five simulations (Sim 1 to Sim 5) are shown as blocks in the figure, each simulation being 200ns long. The grey shaded areas show the residence time of the system in the closed state.

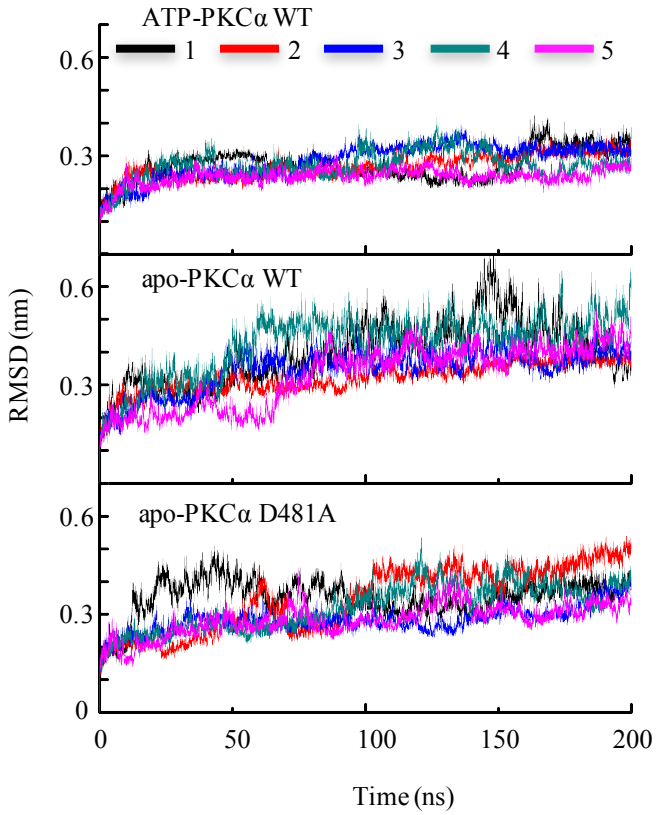

Figure S4: Root mean square deviation (RMSD) in nm, of the Cα atoms of the catalytic domain of PKCα, plotted over 200 ns of 5 parallel simulations of PKCα for apo-wild type, D481A mutant, and wild type PKCα bound to ATP. The RMSD converges at the end of 200ns in most of the simulations.

References

(1) Wagner, J., von Matt, P., Sedrani, R., Albert, R., Cooke, N., Ehrhardt, C., Geiser, M., Rummel, G., Stark, W., Strauss, A., Cowan-Jacob, S. W., Beerli, C., Weckbecker, G., Evenou, J.-P., Zenke, G., and Cottens, S. (2009) Discovery of 3-(1 H -Indol-3-yl)-4-[2-(4-methylpiperazin-1-yl)quinazolin-4-yl]pyrrole-2,5-dione (AEB071), a Potent and Selective Inhibitor of Protein Kinase C Isotypes. *J. Med. Chem. 52*, 6193–6196.
(2) Webb, B., and Sali, A. (2014) Comparative Protein Structure Modeling Using MODELLER. *Curr. Protoc. Bioinforma. 47*, 5.6.1-5.6.32.
(3) Leonard, T. A., Różycki, B., Saidi, L. F., Hummer, G., and Hurley, J. H. (2011) Crystal Structure and Allosteric Activation of Protein Kinase C βII. *Cell 144*, 55–66.
(4) George, D. M., Breinlinger, E. C., Argiriadi, M. A., Zhang, Y., Wang, J., Bansal-Pakala, P., Duignan, D. B., Honore, P., Lang, Q., Mittelstadt, S., Rundell, L., Schwartz, A., Sun, J., and Edmunds, J. J. (2015) Optimized Protein Kinase Cθ (PKCθ) Inhibitors Reveal Only Modest Anti-inflammatory Efficacy in a Rodent Model of Arthritis. *J. Med. Chem. 58*, 333–346.
(5) Kallan, N. C., Spencer, K. L., Blake, J. F., Xu, R., Heizer, J., Bencsik, J. R., Mitchell, I. S., Gloor, S. L., Martinson, M., Risom, T., Gross, S. D., Morales, T. H., Wu, W.-I., Vigers, G. P. A., Brandhuber, B. J., and Skelton, N. J. (2011) Discovery and SAR of spirochromane Akt inhibitors. *Bioorg. Med. Chem. Lett. 21*, 2410–2414.
(6) Durzynska, I., Xu, X., Adelmant, G., Ficarro, S. B., Marto, J. A., Sliz, P., Uljon, S., and Blacklow, S. C. (2017) STK40 Is a Pseudokinase that Binds the E3 Ubiquitin Ligase COP1. *Structure 25*, 287–294.
(7) Komander, D., Kular, G. S., Bain, J., Elliott, M., Alessi, D. R., and van Aalten, D. M. F. (2003) Structural basis for UCN-01 (7-hydroxystaurosporine) specificity and PDK1 (3-phosphoinositide-dependent protein kinase-1) inhibition. *Biochem. J. 375*, 255–262.
(8) Pemovska, T., Johnson, E., Kontro, M., Repasky, G. A., Chen, J., Wells, P., Cronin, C. N., McTigue, M., Kallioniemi, O., Porkka, K., Murray, B. W., and Wennerberg, K. (2015) Axitinib effectively inhibits BCR-ABL1(T315I) with a distinct binding conformation. *Nature 519*, 102–105.
(9) Sievers, F., Wilm, A., Dineen, D., Gibson, T. J., Karplus, K., Li, W., Lopez, R., McWilliam, H., Remmert, M., Söding, J., Thompson, J. D., and Higgins, D. G. (2011) Fast, scalable generation of high-quality protein multiple sequence alignments using Clustal Omega. *Mol. Syst. Biol. 7*, 539.
(10) Wagner, J., von Matt, P., Sedrani, R., Albert, R., Cooke, N., Ehrhardt, C., Geiser, M., Rummel, G., Stark, W., Strauss, A., Cowan-Jacob, S. W., Beerli, C., Weckbecker, G., Evenou, J.-P., Zenke, G., and Cottens, S. (2009) Discovery of 3-(1H-Indol-3-yl)-4-[2-(4-methylpiperazin-1-yl)quinazolin-4-yl]pyrrole-2,5-dione (AEB071), a Potent and Selective Inhibitor of Protein Kinase C Isotypes. *J. Med. Chem. 52*, 6193–6196.
(11) Elkins, J. M., Amos, A., Niesen, F. H., Pike, A. C. W., Fedorov, O., and Knapp, S. (2009) Structure of dystrophia myotonica protein kinase. *Protein Sci. 18*, 782–791.
(12) Xu, Z.-B., Chaudhary, D., Olland, S., Wolfrom, S., Czerwinski, R., Malakian, K., Lin, L., Stahl, M. L., Joseph-McCarthy, D., Benander, C., and others. (2004) Catalytic domain crystal structure of protein kinase C-θ (PKCθ). *J. Biol. Chem. 279*, 50401–50409.
(13) Takimura, T., Kamata, K., Fukasawa, K., Ohsawa, H., Komatani, H., Yoshizumi, T., Takahashi, I., Kotani, H., and Iwasawa, Y. (2010) Structures of the PKC-ι kinase domain in its ATP-bound and apo forms reveal defined structures of residues 533–551 in the C-terminal tail and their roles in ATP binding. *Acta Crystallogr. Sect. D Biol. Crystallogr. 66*, 577–583.
(14) Berendsen, H. J. C., van der Spoel, D., and van Drunen, R. (1995) GROMACS: A message-passing parallel molecular dynamics implementation. *Comput. Phys. Commun. 91*, 43–56.
(15) Schmid, N., Eichenberger, A. P., Choutko, A., Riniker, S., Winger, M., Mark, A. E., and Van Gunsteren, W. F. (2011) Definition and testing of the GROMOS force-field versions 54A7 and 54B7. *Eur. Biophys. J. 40*, 843–856.
(16) Hansson, T., Nordlund, P., and Åqvist, J. (1997) Energetics of nucleophile activation in a protein tyrosine phosphatase. *J. Mol. Biol. 265*, 118–127.
(17) Darden, T., York, D., and Pedersen, L. (1993) Particle mesh Ewald: An N·log(N) method for Ewald sums in large systems. *J. Chem. Phys. 98*, 10089–10092.
(18) Martyna, G. J., Klein, M. L., and Tuckerman, M. (1992) Nosé–Hoover chains: The canonical ensemble via continuous dynamics. *J. Chem. Phys. 97*, 2635–2643.
(19) Parrinello, M., and Rahman, A. (1981) Polymorphic transitions in single crystals: A new molecular dynamics method. *J. Appl. Phys. 52*, 7182–7190.
(20) Schüttelkopf, A. W., and van Aalten, D. M. F. (2004) PRODRG : a tool for high-throughput crystallography of protein–ligand complexes. *Acta Crystallogr. Sect. D Biol. Crystallogr. 60*, 1355–1363.
(21) Bochevarov, A. D., Harder, E., Hughes, T. F., Greenwood, J. R., Braden, D. A., Philipp, D. M., Rinaldo, D., Halls, M. D., Zhang, J., and Friesner, R. A. (2013) Jaguar: A high-performance quantum chemistry software program with strengths in life and materials sciences. *Int. J. Quantum Chem. 113*, 2110–2142.
(22) Humphrey, W., Dalke, A., and Schulten, K. (1996) VMD: Visual molecular dynamics. *J. Mol. Graph. 14*, 33–38.
(23) Lee, S., Devamani, T., Song, H. D., Sandhu, M., Larsen, A., Sommese, R., Jain, A., Vaidehi, N., and Sivaramakrishnan, S. (2017) Distinct structural mechanisms determine substrate affinity and kinase activity of protein kinase Cα. *J. Biol. Chem. 292*, 16300–16309.
(24) Vaidehi, N., and Jain, A. (2015) Internal coordinate molecular dynamics: a foundation for multiscale dynamics. *J. Phys. Chem. B 119*, 1233–42.
(25) Sommese, R. F., and Sivaramakrishnan, S. (2016) Substrate Affinity Differentially Influences Protein Kinase C Regulation and Inhibitor Potency. *J. Biol. Chem. 291*, 21963–21970.
(26) Sivaramakrishnan, S., and Spudich, J. A. (2011) Systematic control of protein interaction using a modular ER/K -helix linker. *Proc. Natl. Acad. Sci. 108*, 20467–20472.
(27) Swanson, C. J., Ritt, M., Wang, W., Lang, M. J., Narayan, A., Tesmer, J. J., Westfall, M., and Sivaramakrishnan, S. (2014) Conserved modular domains team up to latch-open active protein kinase Cα. *J. Biol. Chem. 289*, 17812–29.
(28) Malik, R. U., Ritt, M., DeVree, B. T., Neubig, R. R., Sunahara, R. K., and Sivaramakrishnan, S. (2013) Detection of G Protein-selective G Protein-coupled Receptor (GPCR) Conformations in Live Cells. *J. Biol. Chem. 288*, 17167–17178.
(29) Sommese, R. F., and Sivaramakrishnan, S. (2016) Substrate affinity differentially influences protein kinase C regulation and inhibitor potency. *J. Biol. Chem. 291*, 21963–21970.
(30) Sommese, R. F., Ritt, M., Swanson, C. J., and Sivaramakrishnan, S. (2017) The role of regulatory domains in maintaining autoinhibition in the multidomain kinase PKCα. *J. Biol. Chem. 292*, 2873–2880.